JOURNAL OF SOLID STATE CHEMISTRY **141,** 411–417 (1998)
ARTICLE NO. SC987963

Crystal Structure and Magnetic Properties of $La_2Co_2O_5$

Ole Henrik Hansteen,* Helmer Fjellvåg,* and Bjørn C. Hauback†

*Department of Chemistry, University of Oslo, N-0315 Oslo, Norway; and †Institutt for Energiteknikk, N-2007 Kjeller, Norway

Received March 9, 1998; in revised form June 29, 1998; accepted June 30, 1998

The crystal structure of $La_2Co_2O_5$ is determined on the basis of high-resolution powder X-ray diffraction and neutron diffraction data. $La_2Co_2O_5$ adopts the brownmillerite-type structure, where single layers of corner-sharing CoO_6-octahedra are connected by layers with chains of corner-sharing CoO_4-tetrahedra running along [100]. Three alternative descriptions of the crystal structure in space groups *Pnma*, *Imma*, and *Ima*2 with slightly different structural distortions and/or atomic disorder are discussed. The unit cell is $a = 544.45(2)$ pm, $b = 1586.89(4)$ pm, 569.22(2) pm, R_{wp}(PXD) = 8.0%, R_{wp}(PND) = 7.3%, R_p(PXD) = 5.3%, R_p(PND) = 5.6% (space group *Pnma*). On reducing $LaCoO_3$ to $La_2Co_2O_5$ there is a 9.8% expansion of the unit cell owing to the increased size of high-spin divalent cobalt atoms, and a significant peak broadening occurs in the high-resolution PXD data. On the basis of powder neutron diffraction data, $La_2Co_2O_5$ is found to order antiferromagnetically (G-type ordering) for temperatures below $T_N = 301 \pm 5$ K. The magnetic moments for the cobalt atoms are $\mu_{oct.} = 3.0 \pm 0.1 \mu_B$ and $\mu_{tetr.} = 2.5 \pm 0.1\ \mu_B$. © 1998 Academic Press

INTRODUCTION

Anion vacancy ordering is common for oxygen deficient perovskites ($AMO_{3-\delta}$), and results in superstructures where the cationic sublattice of the perovskite is left essentially unchanged. The coordination of some or all the M atoms, which usually is a transition element, decreases from octahedral to typically square pyramidal, tetrahedral, or square planar, e.g., $Ca_2Mn_2O_5$ (1), $Ca_2Fe_2O_5$ (2), and $La_2Ni_2O_5$ (3), respectively. The type of vacancy ordering is strongly dependent on the nature of the transition element. $A_2M_2O_5$ compounds with tetrahedral coordination of M often adopt the brownmillerite-type structure. Here the anion vacancy ordering leads to the formation of layers with chains of corner-sharing MO_4-tetrahedra connecting single perovskite layers of corner-sharing MO_6-octahedra.

Reduction of perovskite type oxides leads to the loss of oxygen, which in most cases is connected with the formation of oxygen vacancies. At low vacancy concentrations clustering occurs, whereas at higher concentrations ordered phases are normally formed. Vidyasagar *et al.* (3) showed that reduction of $LaCoO_3$ at low temperatures leads to the ordered phase $La_2Co_2O_5$ for which the brownmillerite type structure was proposed. The lowering of the valence state of cobalt from three to two is expected to give rise to considerably different electronic and magnetic properties. The present study reports on a detailed determination of the crystal and magnetic structures of $La_2Co_2O_5$ based on a combined profile analysis of high-resolution powder X-ray diffraction data collected at ESRF and powder neutron diffraction data.

EXPERIMENTAL

Synthesis

$La_2Co_2O_5$ was prepared by isothermal reduction of single-phase $LaCoO_3$. $LaCoO_3$ was first prepared by a citrate precursor method (4). The starting materials for the synthesis were La_2O_3 (99.99% Molycorp), $Co(CH_3COO)_2 \cdot 4H_2O$ (> 99% Fluka), and citric acid monohydrate, $C_3H_4(OH)(COOH)_3 \cdot H_2O$ (> 99.8% Riedel-de Haën). Single-phase $LaCoO_3$ was obtained after calcination in air at 1300 K for 110 h. Phase purity was assured from powder X-ray diffraction. The isothermal reduction of $LaCoO_3$ to $La_2Co_2O_5$ was performed in sealed silica glass ampoules at 673 K using chips of Zr (99.5% A. D. Mackay Inc.) as reducing agent (cf. Ref. 5 for further details). The ampoules were opened in an argon-filled glovebox [$p(O_2)$ and $p(H_2O) < 1$ ppm]. Care was taken to ensure inert atmosphere during storage, handling, and subsequent characterization of specimens.

Powder Diffraction

Room-temperature powder X-ray diffraction (PXD) data were collected for all samples with a Guinier–Hägg camera using Si as an internal standard ($a = 543.1065$ pm). The sample holders were filled with oil and sealed with Scotch tape on top and bottom. The sample adhered to the bottom tape, which prevented it from dispersing into the oil. Both Cr$K\alpha_1$ (detection limit for impurities ca. 0.3 wt% (6)) and Cu$K\alpha_1$ radiation were used. Unit-cell dimensions were

0022-4596/98 $25.00

determined by least-squares calculations using the program UNITCELL (7). Synchrotron (SR) PXD data were collected for $La_2Co_2O_5$ with the powder diffractometer in the Debye–Scherrer mode at the Swiss Norwegian Beam Line (BM1) at ESRF (Grenoble). The sample was contained in a sealed and rotating glass capillary with diameter 0.2 mm (chosen for reducing absorption). Intensity data were collected at 298 K between $2\theta = 3.5^\circ$ and 63° in steps of $\Delta(2\theta) = 0.008^\circ$, $\lambda = 109.803$ pm. Powder neutron diffraction (PND) data were collected for $La_2Co_2O_5$ with the two-axis powder diffractometer OPUS at the JEEP II reactor, Kjeller (Norway). A cylindrical sample holder of aluminum, carefully sealed with an indium washer, was used. Intensity data were collected at 10 and 298 K between $2\theta = 7^\circ$ and 102° in steps of $\Delta(2\theta) = 0.05^\circ$, $\lambda = 182.5$ pm. The GSAS program package (8) was used for the combined Rietveld-type profile refinements of powder synchrotron X-ray and neutron diffraction data collected at 298 K. Table 1 summarizes the characteristic features of the data sets and the variable parameters entering the least-squares refinements. For the synchrotron PXD data the background was modeled by a power series in $Q^{2n}/n!$ and $n!/Q^{2n}$, where $Q = 2\pi/d$ (GSAS function no. 6). The peak shape was modeled by a pseudo-Voigt function. For the PND data the background was modeled by cosine Fourier series polynomials, and the peak shape was modeled by a Gaussian function. The scattering lengths $b_{La} = 8.27$ fm, $b_{Co} = 2.53$ fm, and $b_O = 5.81$ fm were taken from the GSAS library. For profile refinement of the PND data collected at 10 K (crystal and magnetic structure) the Hewat version (9) of the Rietveld program (10) was used.

TABLE 1
Characteristic Features of the Powder Synchrotron X-Ray (298 K) and Neutron Diffraction (10, 298 K) Data Sets for $La_2Co_2O_5$ and a List of Parameters Entering the Profile Refinements

	PXD(SR)		PND	
Measured data points	7424		1764	
Reflections (*hkl*)	244		178	
λ (pm)	109.803		182.5	
Scale factor	1		1	
Zero point	1		1	
Profile parameters	6		3	
Unit-cell dimensions		3[a]		
Positional parameters		13[a]		
Isotropic displacement factors		3[a]		
Magnetic components			(4)[b]	
Background coefficients	15		12	
Refinable parameters	23	+ 19	+ 17	= 59

[a]Common parameters for PXD(SR) and PND in the combined refinements.

[b]Only refined for the 10 K data.

Magnetic Measurements

Magnetic susceptibility data were measured by a Quantum Design SQUID-magnetometer (MPMS) in the temperature range 2–300 K for magnetic fields (H) up to 40.0 kOe. All samples were zero field cooled and the temperature dependence of the magnetic susceptibility was measured on heating. A Faraday balance was used for susceptibility measurements performed on heating in the temperature range 300–970 K; $H \leq 7.0$ kOe. The samples were held in evacuated and sealed spherical silica glass ampoules. The measured magnetic susceptibility was corrected for diamagnetic contribution from the sample container and from core electrons.

RESULTS AND DISCUSSION

(i) Crystal Structure

The Guinier–Hägg PXD pattern at 298 K for $La_2Co_2O_5$ was indexed satisfactorily using the primitive orthorhombic unit cell description of a brownmillerite-type crystal structure. The description by Berggren (2) for orthorhombic $Ca_2Fe_2O_5$ (space group *Pnma*) was used as a starting model for the combined Rietveld type refinements of the synchrotron PXD and the PND data. The results are given in Tables 2–4. The unit-cell dimensions are somewhat lower than reported by Vidyasagar *et al.* (3) The crystal structure, Fig. 1, is a layered arrangement consisting of single perovskite-type layers of corner-sharing CoO_6-octahedra, Co(1), parallel to the *ac*-plane of the unit-cell. These layers are connected by "layers" consisting of chains of corner-sharing

TABLE 2
Unit-Cell Data for $La_2Co_2O_5$ and Reliability Factors

		298 K	10 K
Crystal system		Orthorhombic	Orthorhombic
Space group		*Pnma*	*Pnma*
a, pm		544.45(2)	543.4(1)
b, pm		1586.89(4)	1582.6(3)
c, pm		569.22(2)	568.7(1)
V, 10^8(pm)^3		4.9180(3)	4.891(2)
Z		4	4
R_p (%)[a]	PXD(SR)	5.3	
	PND	5.6	14.3[b]
R_{wp} (%)[a]	PXD(SR)	8.0	
	PND	7.3	22.0
R_{exp} (%)[a]	PXD(SR)	5.7	
	PND	5.2	14.9
χ^2		1.97	2.17

Note. Calculated standard deviations in parentheses.

[a]$R_p = 100(\sum |I_O - I_C|/\sum I_O)$, $R_{wp} = 100(\sum w(I_O - I_C)^2/\sum w I_O^2)^{-1/2}$, $R_{exp} = R_{wp}/\sqrt{\chi^2}$ according to Ref. (8) (298 K) and Refs. (9, 10) (10 K).

[b]Combined refinement, crystallographic ($R_N = 14.5\%$) and magnetic ($R_M = 12.6\%$).

TABLE 3
Fractional Atomic Coordinates for $La_2Co_2O_5$ at 298 K

Atom	Wyckoff site[a]	x	y	z
La(1)	8*d*	0.5002(8)	0.11035(9)	0.0148(4)
Co(1)	4*a*	0	0	0
Co(2)	4*c*	0.972(2)	0.25	0.936(1)
O(1)	8*d*	0.242(1)	0.9851(3)	0.247(1)
O(2)	8*d*	0.000(1)	0.1418(2)	0.0691(6)
O(3)	4*c*	0.599(1)	0.25	0.883(1)

Note. Calculated standard deviations in parentheses. Space group *Pnma*. Isotropic displacement factors (B_{iso} in $10^4 pm^2$): $B_{iso}(La) = 2.23(5)$, $B_{iso}(Co) = 0.4(1)$, $B_{iso}(O) = 1.43(8)$.
[a] 4*a* (0, 0, 0), 4*c* (x, $\frac{1}{4}$, z), 8*d* (x, y, z).

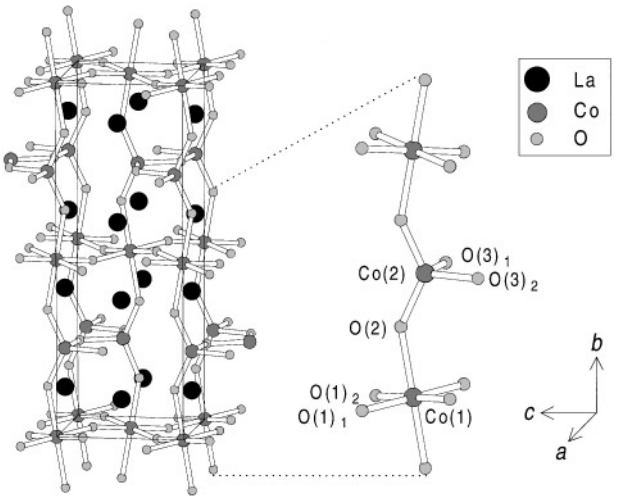

FIG. 1. Crystal structure of $La_2Co_2O_5$. Space group *Pnma*.

CoO_4-tetrahedra, Co(2), running parallel to the *a*-axis. The unit cell comprises two such chains, which are translated by $(\bar{b}/2 + \bar{c}/2)$. The chains are related by centrosymmetry in space group *Pnma*. This space group allows all atoms to be placed in fully occupied positions (cf. Table 3). This structural model for $La_2Co_2O_5$ gave a quite reasonable fit to the observed data, see the calculated and difference profiles in Fig. 2. The not perfect fit to the PXD(SR) data is ascribed to a noncomplete powder situation owing to the thin capillaries used.

In describing the structure for $La_2Co_2O_5$, two alternative body-centered descriptions were examined which implies slightly different structural distortions and also atomic disorder. The first model refers to the space group *Imma* description of $Sr_2Fe_2O_5$ (12). This model requires Co(2) and O(3) to be randomly distributed over half-occupied 8*i* (x, $\frac{1}{4}$, z) positions. However, this model gave no significant improvement of the *R*-factors (PXD(SR): $R_p = 5.3\%$, $R_{wp} = 7.9\%$; PND: $R_p = 5.6\%$, $R_{wp} = 7.4\%$). The possibility of fixing Co(2) and O(3) in fourfold positions 4*e* (0, $\frac{1}{4}$, z) can be excluded since it leads to severe distortions of the CoO_4-tetrahedra and a poor fit. The second model is based on space group *Ima*2. All atoms can be placed in fully occupied positions, and satisfactory tetrahedral coordination of Co(2) is provided. However, the tetrahedral chains are not related by centrosymmetry, and more irregular octahedra are obtained, e.g., with a significant deviation from 180° of the O(2)–Co(1)–O(2) angle (176.2°). The model gave no significant improvement of the *R*-factors (PXD: $R_p = 5.4\%$, $R_{wp} = 8.0\%$; PND: $R_p = 5.7\%$, $R_{wp} = 7.3\%$). There is no doubt that $La_2Co_2O_5$ basically adopts the brownmillerite-type structure. However, the rather equivalent fit obtained for the refinements according to the space groups *Pnma*, *Imma*, and *Ima*2 shows that there is still some ambiguity concerning the space group assignment.

The peak shape of the PXD(SR) data for $La_2Co_2O_5$ (FWHM = 0.049°) is compared to that for $LaCoO_3$ (FWHM = 0.028°) in Fig. 3. Clearly, the $La_2Co_2O_5$ sample which was prepared by low temperature reduction has significantly broader reflections than $LaCoO_3$, which was equilibrated at higher temperatures and used as the precursor for the reduction. Similar peak broadening occurs for the related low temperature reduced phases $La_3Co_3O_8$ and $La_4Co_3O_9$ (5, 11). The peak broadening may stem from particle strain, which is related to the expansion of the crystal structure occuring upon reduction (see below),

TABLE 4
Selected Interatomic Distances and Bond Angles for $La_2Co_2O_5$ at 298 K

Distances (pm)			Angles (°)	
		Octahedron		
$Co(1)–O(1)_1$	(×2)	194(2)	$O(1)_1–Co(1)–O(1)_2$	93.4 (1)
$Co(1)–O(1)_2$	(×2)	203(1)	O(1)–Co(1)–O(2)	89.7 (5)
Co(1)–O(2)	(×2)	228 (1)		
		Tetrahedron		
Co(2)–O(2)	(×2)	188(1)	O(2)–Co(2)–O(2)	131.6(4)
$Co(2)–O(3)_1$		205(1)	$O(3)_1–Co(2)–O(2)$	98.1(4)
$Co(2)–O(3)_2$		195(1)	$O(3)_2–Co(2)–O(2)$	110.2(3)
			$O(3)_1–Co(2)–O(3)_2$	102.4(4)
La–O	240–279, 336 (1)		8 + 1	
Polyhedra tilt angles (°)				
Co(1)–O(2)–Co(2)	146.0(3)			
Co(1)–O(1)–Co(1)	166.3(2)			
Co(2)–O(3)–Co(2)	119.3(4)			

Note. Calculated standard deviations in parentheses. Atom numbers refer to Fig. 1.

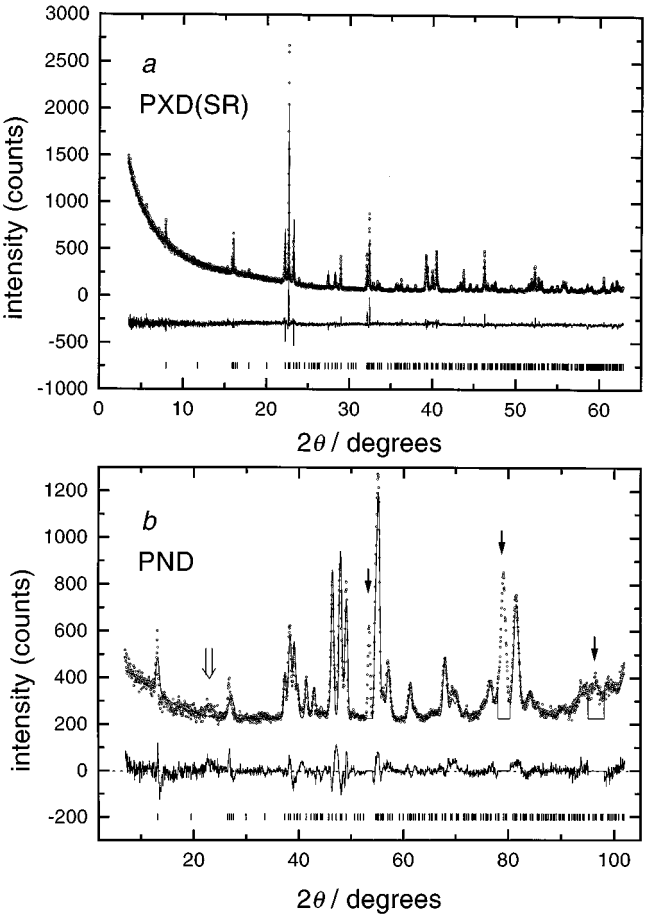

FIG. 2. (a) Synchrotron PXD ($\lambda = 109.803$ pm) and (b) PND ($\lambda = 182.5$ pm) profiles for $La_2Co_2O_5$ at 298 K. Experimental points marked by circles, full line marks calculated profile, lower full line marks difference plot, vertical bars marks positions for Bragg reflections. Solid arrows in the PND pattern mark excluded reflections from the aluminum container, open arrow marks weak magnetic scattering.

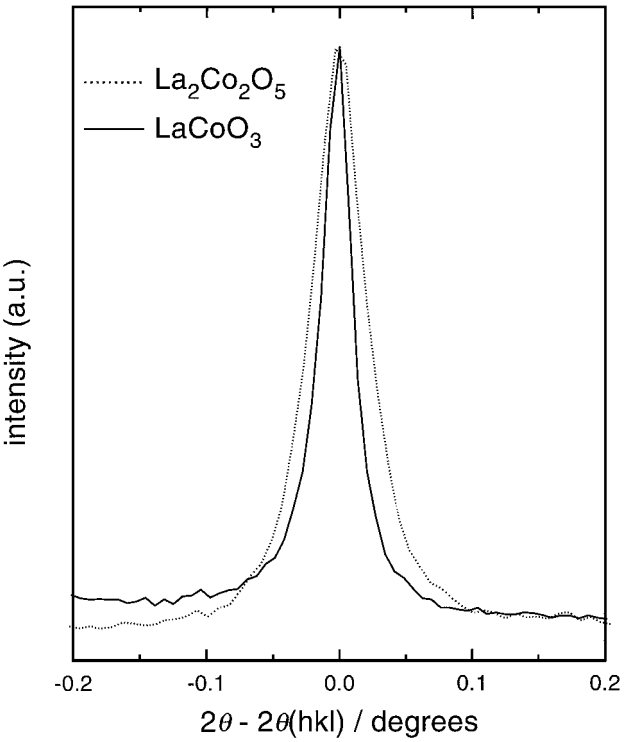

FIG. 3. Peak shape of reflections from PXD(SR) data for $La_2Co_2O_5$ (dotted line) and $LaCoO_3$ (full line). Reflections with Miller indices (200) for $La_2Co_2O_5$ at $d = 279.19$ pm and (104) for $LaCoO_3$ at $d = 268.70$ pm are plotted.

combined with possible disordered intergrowth of units of related phases $La_nCo_nO_{3n-1}$ with different oxygen content; i.e., $n > 2$. The apparent particle size distribution is constant as seen by scanning electron microscopy. However, peak broadening due to the formation of microdomains on symmetry lowering cannot be ruled out. On the other hand, this is not the cause for peak broadening during reduction of $La_4Co_3O_{10}$ to $La_4Co_3O_9$ since no such symmetry lowering occurs.

A closer inspection of Fig. 1 shows that the perovskite-type cationic arrangement is essentially retained in the reduced-phase $La_2Co_2O_5$. The unit-cell dimensions for orthorhombic $La_2Co_2O_5$ are compared with relevant dimensions for rhombohedral $LaCoO_3$ (13) in Table 5. On reducing $LaCoO_3$ to $La_2Co_2O_5$ there is a 9.8% expansion of the unit-cell volume. For comparison, the expansion is 5.5% upon reduction of $LaCoO_3$ to $La_3Co_3O_8$. The main source for the volume expansion is the increased size of divalent, high-spin cobalt atoms, $Co^{II}(d^7)$, relative to trivalent, low-spin $Co^{III}(d^6)$. The small displacements of the Co(2) and the oxygen atoms together with the expansion of $\bar{c}$ reduce the distortions of the CoO_4-tetrahedra. At the same time considerable tilting of the CoO_6-octahedra occurs. Despite the displacements, the tetrahedra are still distorted, especially along [010] as shown by the large O(2)–Co(2)–O(2) angle and the short Co(2)–O(2) interatomic distance (Table 4). Furthermore, the CoO_6-octahedra are

TABLE 5
Comparison of Unit-Cell Dimensions for Orthorhombic $La_2Co_2O_5$ (a, b, c) and Rhombohedral $LaCoO_3$ (a_R, a_C, a_H)

$La_2Co_2O_5$		$LaCoO_3$[a]	
a (pm)	544.45	a_R (pm)	537.78
b (pm)	1586.89	$4a_C$ (pm)	1530.39
c (pm)	569.22	a_H (pm)	544.25
V (10^8pm^3)	4.918	V (10^8pm^3)	4.479

[a]Subscripts R and H correspond to the rhombohedral and hexagonal setting of the unit cell of $LaCoO_3$ (13), respectively. a_C refers to the Co–Co interatomic distance which corresponds to the a-axis of the cubic perovskite-type unit cell.

TABLE 6
Calculated Lanthanum and Cobalt Bond Valences (v_i) for Phases in the La–Co–O System[a]

	Co^{II}-fraction	v_{Co} (tetrahedral)	v_{Co} (octahedral)	v_{La} (12 coordinated)	v_{La} (9 coordinated)	Ref.
$LaCoO_3$	0	—	3.21	3.17	—	(13)
$La_4Co_3O_{10}$	1/3	—	2.84, 2.92, 3.02, 3.22	2.98, 3.03	2.98, 3.11	(15)
$La_3Co_3O_8$	2/3	1.92	2.44, 3.16	2.73	2.81, 3.03	(5)
$La_2Co_2O_5$	1	2.08	2.23	—	2.64	this work
$La_4Co_3O_9$	1	1.92	2.27	—	2.65, 2.75	(11)
La_2CoO_4	1	—	2.82	—	2.52	(16)

[a] $v_i = \sum \exp[(D_i - d_i)/0.37]$ (cf. Ref. 14), $D^{II}_{Co} = 1.692$, $D^{III}_{Co} = 1.700$, $D^{III}_{La} = 2.172$, d_i = experimentally determined interatomic distances.

significantly elongated along [010], and the ninefold coordination of oxygen around lanthanum is irregular.

Bond valences (14) for La and Co were calculated for $La_2Co_2O_5$ and all other ternary phases in the La–Co–O system for comparison, see Table 6. Common to all these phases is that the loss of oxygen due to the reduction of Co^{III} to Co^{II}, is accompanied by a reduction of the coordination number of lanthanum from 12 to 9. The bond valences for trivalent lanthanum are significantly lower than expected for the phases $La_2Co_2O_5$, $La_4Co_3O_9$, and La_2CoO_4, with solely divalent cobalt and nine-coordinated La. The low lanthanum bond valences possibly indicate that ninefold coordination is unfavorable for La. The increasing (and more favorable with respect to valence) coordination for La in the Co^{III}-containing phases may act as an additional driving force for the oxidation reaction.

All the structural features discussed for $La_2Co_2O_5$ are common for several $A_2M_2O_5$ compounds with the brownmillerite structure, e.g., $Ca_2Fe_2O_5$ (2), $Sr_2Fe_2O_5$ (12), Sr_2CoFeO_5 (17), and $Sr_2In_2O_5$ (18). For $Sr_2Co_2O_5$ the brownmillerite structure is obtained only by quenching from high temperatures, whereas the low-temperature crystal structure is rhombohedral. This deviating feature for $Sr_2Co_2O_5$ has been discussed to result from a larger size difference between the two cations (19–20). Whereas these and most other brownmillerite-type phases are of the type $A^{II}_2M^{III}_2O_5$, the present phase is different with $La^{III}_2Co^{II}_2O_5$.

(*ii*) *Magnetic Properties*

The powder neutron diffraction study showed that additional magnetic reflections gain intensity rapidly on decreasing the temperature below ambient, see Fig. 4. There

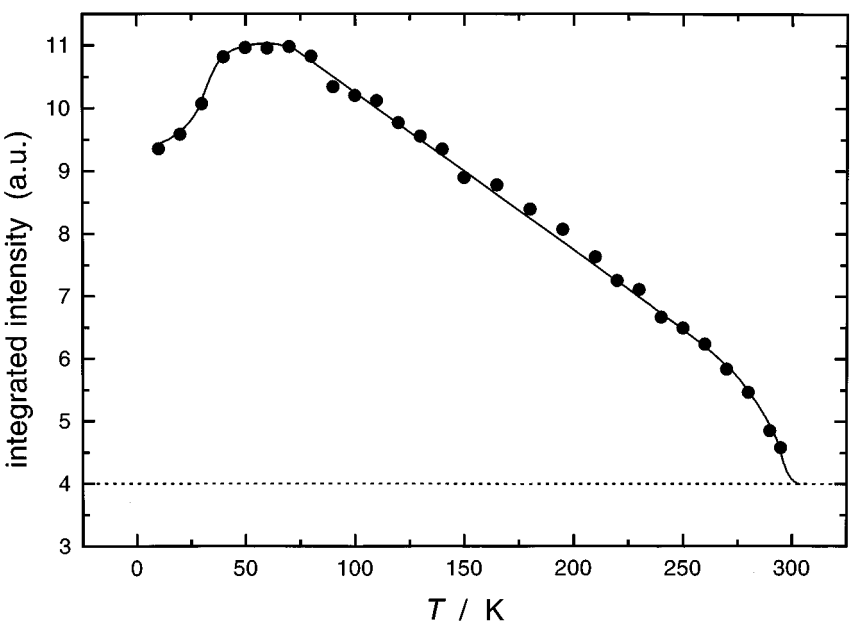

FIG. 4. Temperature dependence of the integrated intensity for the overlapping magnetic reflections (021) and (120). Dashed line represents the background level. Fully drawn line is a guide to the eye.

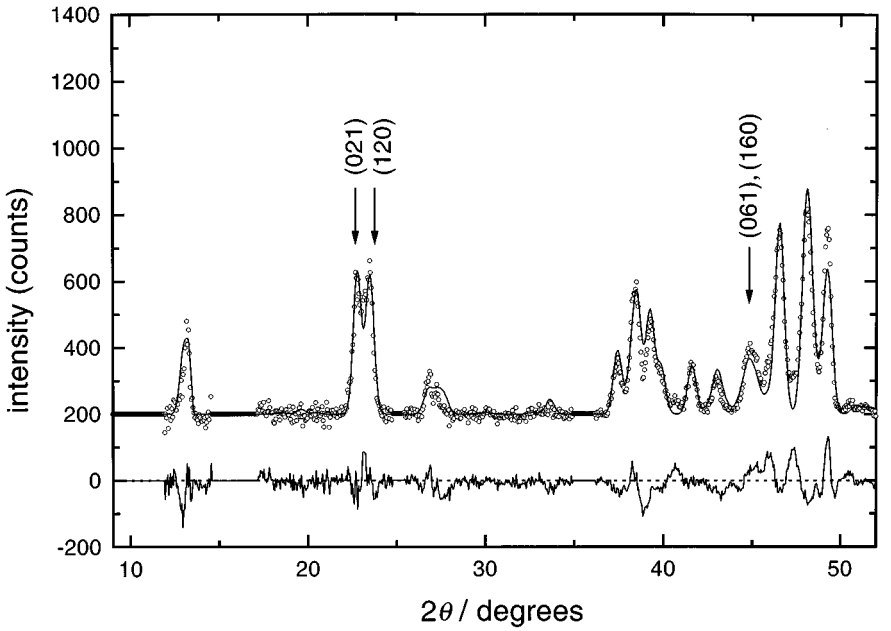

FIG. 5. Part of the observed PND profile for $La_2Co_2O_5$ at 10 K ($\lambda = 182.5$ pm). Miller indices for magnetic reflections are given. Experimental points marked by open circles, full line marks the calculated profile, and lower full line marks the difference plot.

is still some observable (diffuse) magnetic scattering at 298 K, slightly above the background level, for the overlapping reflections (021) and (120), cf. open arrow in Fig. 2b. The antiferromagnetic ordering temperature $T_N = 301 \pm 5$ K is estimated by extrapolation of the temperature dependence of the integrated intensity (Fig. 4) to the background level. All the magnetic reflections could be indexed on the crystallographic unit cell. Magnetic coupling for transition elements in the perovskite type oxides occurs typically through cation–anion–cation interactions (21). Assuming the Co^{II}–O–Co^{II} interactions to be antiferromagnetic in nature both for the tetrahedrally and octahedrally coordinated cobalt atoms, a number of possible models were tested. The fit of the PND data to a model where the magnetic moments of all cobalt atoms are antiferromagnetically oriented relatively to the six nearest neighboring cobalt atoms (G-type ordering) are given in Fig. 5. The obtained magnetic *R*-factor (R_M) is 12.6%. The antiferromagnetic ordering for $La_2Co_2O_5$ is shown in Fig. 6. The refined magnetic moments are $\mu_{oct.} = 3.0 \pm 0.1\ \mu_B$ for Co(1) and $\mu_{tetr.} = 2.5 \pm 0.1\ \mu_B$ for Co(2), both moments beeing oriented parallel to [101]. These values correspond fairly well to the expected value for high-spin $Co^{II}(d^7, S = 3/2)$. Similar strong G-type antiferromagnetic coupling is reported for several other brownmillerite phases, $Ca_2Fe_2O_5$ (22), Ca_2FeAlO_5 (23), $Sr_2Fe_2O_5$ (12), Sr_2CoFeO_5 (17), and $Sr_2Co_2O_5$ (24), all with $Fe^{III}(d^5)$ or $Co^{III}(d^6)$ in the high-spin state. For all the latter phases the magnetic moments are oriented parallel to either [100] or [001].

The measured magnetization (M_g) of $La_2Co_2O_5$ (Fig. 7) shows several indications for a ferromagnetic impurity phase not detectable by PXD. The impurity is most probably minor amounts of metallic cobalt precipitated during the reduction. The magnetization is field dependent at all measured temperatures, and a small hysteresis is apparent

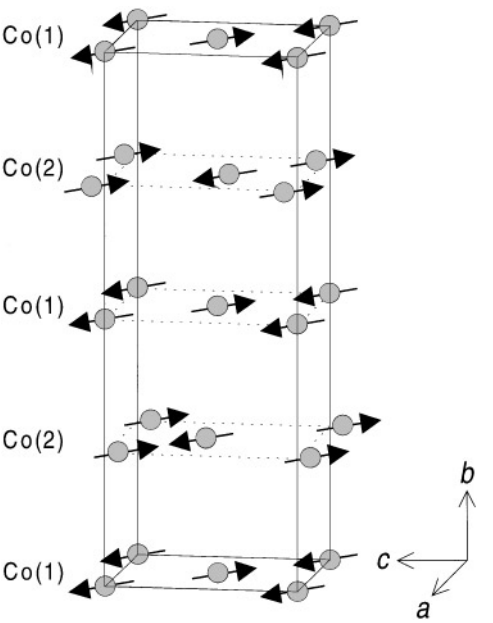

FIG. 6. Antiferromagnetic order in $La_2Co_2O_5$. Only Co atoms are shown.

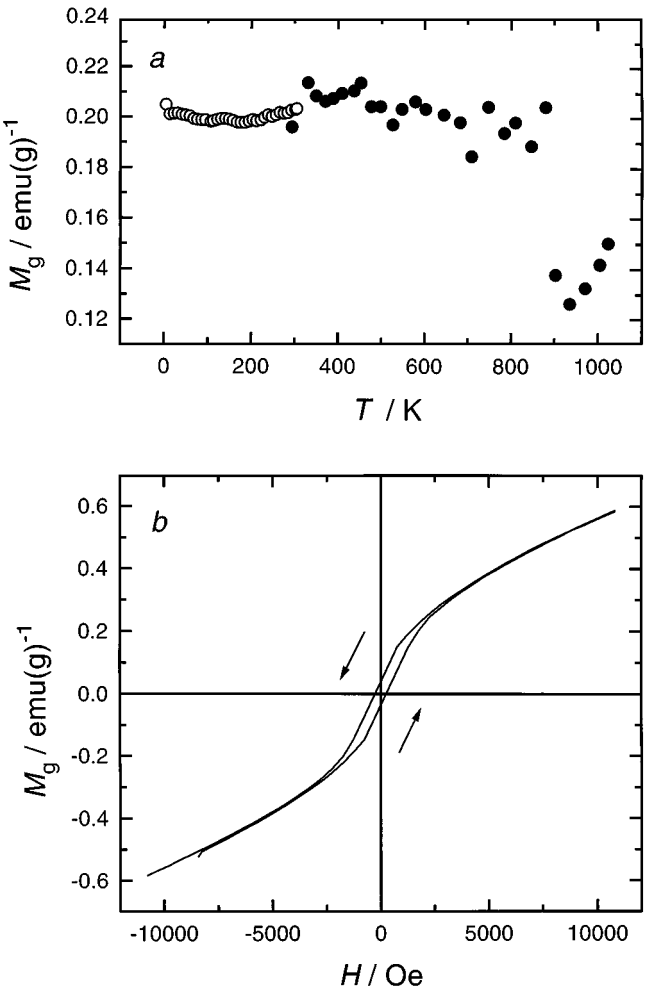

FIG. 7. (a) Temperature dependence of the magnetization (M_g) for $La_2Co_2O_5$ between 5 and 1000 K (SQUID $T < 300$ K, Faraday $T > 300$ K), (b) field dependence of M_g for $La_2Co_2O_5$ at 5 K.

in the $M_g(H)$ curve (Fig. 7b). Judged from the low magnetisation, the ferromagnetic component is small and it is saturated in moderate fields. The present results are in accordance with the magnetization measurements of Sis *et al.* (25) on reduced samples of $LaCoO_{3-\delta}$. The magnetization is apparently temperature independent in low fields for $T < 880$ K (Fig. 7a), as typically observed for ferromagnetic materials at temperatures well below their disordering temperature (for bulk Co metal T_C is 1388 K (26)). The abrupt drop in $M_g(T)$ at 880 K marks the onset of the decomposition of $La_2Co_2O_5$ into La_2CoO_4 and CoO. The decomposition was confirmed by PXD and differential thermal analysis (5). Poor reproducibility of the magnetization between different samples suggests inhomogenous distribution of the ferromagnetic impurity phase throughout the bulk sample. The existence of binary cobalt oxides as precursor impurities for formation of Co(s) cannot be ruled out (27). However, it appears also plausible that Co(s) is formed owing to surface or inhomogenous reduction, or simply by a minor excess of the reducing agent.

ACKNOWLEDGMENTS

This work has received financial support from the Research Council of Norway. The skillful assistance from the project team at the Swiss–Norwegian Beam Line, ESRF, is gratefully acknowledged (Contribution No. 98.10 from the Swiss–Norwegian Beam Line at ESRF).

REFERENCES

1. C. N. R. Rao, J. Gopalakrishnan, and K. Vidyasagar, *Indian J. Chem. A* **23,** 265 (1984).
2. J. Berggren, *Acta Chem. Scand.* **25,** 3616 (1971).
3. K. Vidyasagar, A. Reller, J. Gopalakrishnan, and C. N. R. Rao, *J. Chem. Soc. Chem. Commun.* **7** (1985).
4. O. H. Hansteen, H. Fjellvåg, and B. C. Hauback, *J. Solid State Chem.* **141,** 212 (1998).
5. O. H. Hansteen, H. Fjellvåg, and B. C. Hauback, *J. Mater. Chem.* **8,** 2081 (1998).
6. B. Gilbu, H. Fjellvåg, and A. Kjekshus, *Acta Chem. Scand.* **48,** 37 (1994).
7. Bengt Noläng, "Program UNITCELL," Department of Chemistry, Uppsala University, Sweden.
8. A. C. Larson and R. B. Von Dreele, "Program GSAS, General Structure Analysis System," LANSCE, MS-H 805, Los Alamos National Laboratory, Los Alamos, NM.
9. A. W. Hewat, "Harwell Report" RRL 73/239 (1973).
10. H. M. Rietveld, *J. Appl. Crystallogr.* **2,** 65 (1969).
11. O. H. Hansteen, H. Fjellvåg, and B. C. Hauback, *J. Mater. Chem.* **8,** 2089 (1998).
12. C. Greaves, A. J. Jacobson, B. C. Toefield, and B. E. F. Fender, *Acta Crystallogr. B* **31,** 641 (1975).
13. G. Thornton, B. C. Toefield, and A. H. Hewat, *J. Solid State Chem.* **61,** 301 (1986).
14. I. D. Brown and D. Altermatt, *Acta Crystallogr. B* **41,** 244 (1985).
15. O. H. Hansteen, H. Fjellvåg, and B. C. Hauback, to be published.
16. U. Lehmann and H. K. Müller-Buschbaum, *Z. Anorg. Allg. Chem.* **470,** 59 (1980).
17. P. D. Battle, T. C. Gibb, and P. Lightfoot, *J. Solid State Chem.* **76,** 334 (1988).
18. R. von Schenck and H. K. Müller-Buschbaum, *Z. Anorg. Allg. Chem.* **395,** 280 (1973).
19. J. Rodriguez and J. M. Gonzalez-Calbet, *Mater. Res. Bull.* **21,** 429 (1986).
20. J. Rodriguez, J. M. Gonzalez-Calbet, J. C. Grenier, J. Pannatier, and M. Anne, *Solid State Commun.* **62,** 231 (1987).
21. J. B. Goodenough, "Magnetism and the Chemical Bond," Wiley, New York, 1963.
22. T. Takeda, Y. Yamaguchi, S. Tomoyoshi, M. Fukase, M. Sugimoto, and H. Watanabe, *J. Phys. Soc. Jpn.* **24,** 446 (1968).
23. R. W. Grant, S. Geller, H. Wiedersich, U. Gonser, and L. D. Fullmer, *J. Appl. Phys.* **39,** 1122 (1968).
24. T. Takeda, Y. Yamaguchi, and H. Watanabe, *J. Phys. Soc. Jpn.* **33,** 970 (1972).
25. L. B. Sis, G. P. Wirtz, and S. C. Sorenson, *J. Appl. Phys.* **44,** 5553 (1973).
26. R. V. Colvin and S. Arajs, *J. Phys. Chem. Solids* **26,** 435 (1965).
27. M. A. Señarís-Rodríguez and J. B. Goodenough, *J. Solid State Chem.* **116,** 224 (1995).